

Orbital-resolved strong-field single ionization of acetyleneQinying Ji,¹ Sen Cui,² Xinyuan You,² Xiaochun Gong,¹ Qiying Song,¹ Kang Lin,¹ Haifeng Pan,¹ Jingxin Ding,¹ Heping Zeng,¹ Feng He,^{2,*} and Jian Wu^{1,†}¹State Key Laboratory of Precision Spectroscopy, East China Normal University, Shanghai 200062, China²Key Laboratory of Laser Plasmas (Ministry of Education) and Department of Physics and Astronomy, Collaborative Innovation Center of IFSA (CICIFSA), Shanghai Jiao Tong University, Shanghai 200240, China

(Received 13 April 2015; published 1 October 2015)

We resolve the strong-field single ionization of acetylene into different channels by differentially normalizing the lateral momenta of the directly escaped electrons from the aligned and antialigned molecules. Distinct electron momentum distributions for different channels are observed using both near-infrared and ultraviolet femtosecond laser pulses with Keldysh parameters close to 1. The results are interpreted as a signature of multiple ionization orbitals.

DOI: [10.1103/PhysRevA.92.043401](https://doi.org/10.1103/PhysRevA.92.043401)

PACS number(s): 33.80.Rv, 34.80.Ht, 42.50.Hz, 42.65.Re

When a molecule is exposed to a near-infrared (NIR) strong laser field, its electrons in the highest occupied molecular orbital (HOMO) are preferentially ionized. Meanwhile, a molecular cation in the ground state is produced. However, some studies showed [1–6] that, even for single-electron ionization, the participation of the next lower-lying orbitals (HOMO- n) cannot be neglected. For instance, it was demonstrated that acetylene-vinylidene isomerization occurs in the excited cation state of $A^2\Sigma_g^+$ via one-electron removal from the HOMO-1 of the acetylene (C_2H_2) [7–9]; whereas the removal of one electron from the HOMO mainly generates the ground-state molecular ion $C_2H_2^+$ [10]. The ultrafast electron ionization initiates the succeeding molecular dynamics and provides a knob to control the ultimate outcome of photon-induced molecular reactions. Since electrons of different orbitals have different binding energies, it is demonstrated [11] that the energy shift of the discretized electron spectra produced by the above-threshold ionization (ATI) in the multiphoton regime probes the participation of various orbitals in the single ionization of molecules. On the other hand, the tunneling probability depends on the profile of the ionizing orbital as approximately described by the molecular Ammosov-Delone-Krainov theory [12,13] or the strong-field approximation (SFA) [14,15]. Thus, the multiorbital dynamics in the tunneling ionization regime can be imaged by the angular distributions of the fragmentized ions [16,17] or the molecular-frame photoelectron angular distributions (MFPADs) [2,5]. To do that, the orientation of the molecular axis needs to be deduced from the ejection directions of the fragmentized ions, a method which is not applicable to channels of nondissociative molecular ions.

The structure of the ionizing orbital is indeed imprinted in the lateral momentum of the directly escaped electron [18] filtered by the tunneling barrier. By differentially normalizing the lateral momenta of the freed electrons from aligned and antialigned molecules, the filter effect of the tunneling barrier can be mostly removed. The structure of the ionizing orbital can hence be clearly revealed, as was recently demonstrated for the nondissociative single ionization of O_2 and N_2 using

NIR ultrashort laser pulses [19]. In this paper, rather than for different molecular species, we resolved various orbitals for different ultimate channels in strong-field single ionization of a C_2H_2 molecule. We found that the nondissociative $C_2H_2^+$ and dissociative (C_2H^+ , H) channels are mainly created by removing one electron from the HOMO and HOMO-1 of the C_2H_2 , respectively. Interestingly, orbital-resolved distinct patterns of electron lateral momenta were observed for both NIR and ultraviolet (UV) ultrashort laser pulses with Keldysh parameters close to 1. The featured patterns of the released electrons are interpreted as the signature of different ionizing orbitals, which show great potential to resolve molecular orbitals for even more complex molecules.

As schematically illustrated in Fig. 1, we performed experimental measurements in the ultrahigh-vacuum chamber of the cold target recoil ion momentum spectroscopy (COLTRIMS) apparatus [20,21]. A femtosecond laser pulse from a multipass amplifier Ti:sapphire laser system (50 fs, 790 nm, 10 kHz femtolasers) was split into an aligning pulse (y polarized) and an ionizing pulse (z polarized). The time delay between the aligning and ionizing pulses, t_i , can be finely adjusted using a computer-controlled motorized stage in the arm of the ionizing pulse. The two pulses were afterwards collinearly recombined and focused by a concave silver mirror onto the supersonic gas jet to impulsively align and singly ionize the molecule, respectively. The molecular jet was produced by coexpanding a mixture of 5% C_2H_2 and 95% He through a $30\ \mu\text{m}$ nozzle under a driving pressure of 1.5 bar. The intensities of the aligning and ionizing pulses in the interaction region were measured to be $I_{a0} = 8 \times 10^{13}$ and $I_{i0} = 1.5 \times 10^{14}$ W/cm², respectively. No ionization by the aligning pulse was observed. The electrons and ions produced by the ionizing pulse were accelerated by a weak electric field (~ 7 V/cm) and detected by two time- and position-sensitive microchannel plate detectors at the opposite ends of the spectrometer. A homogeneous magnetic field (~ 8.3 G) was used to guide the freed electrons to ensure detection efficiency in the whole 4π solid angle. The three-dimensional momenta of the detected electrons and ions were reconstructed during the off-line data analysis. Atomic units (a.u.) are used throughout unless otherwise specified.

In our experiments, the event rates of the ion and electron from the two detectors are 0.1 ions and 0.22 electrons per laser shot, respectively. Governed by the intrinsic properties of the

*fhe@sjtu.edu.cn

†jwu@phy.ecnu.edu.cn

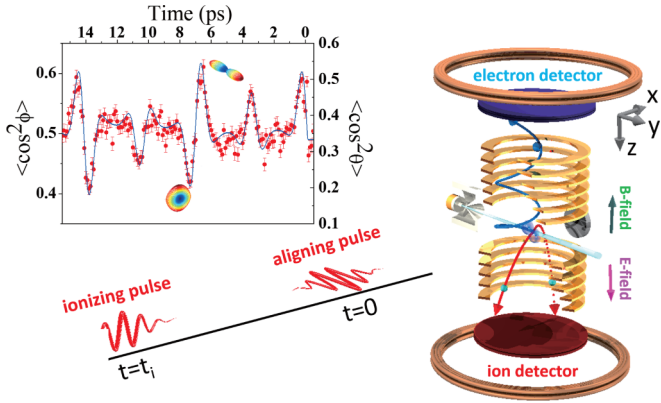


FIG. 1. (Color online) Schematic diagram of the experimental setup. Molecules in the supersonic gas jet are impulsively aligned by a y -polarized aligning pulse and subsequently ionized by a z -polarized ionizing pulse. The ions and electrons are detected by two time- and position-sensitive detectors at the opposite ends of the spectrometer in the ultrahigh-vacuum apparatus of COLTRIMS. The insets show the measured time-dependent evolution of $\langle \cos^2 \phi \rangle$ (red circles) and the simulated $\langle \cos^2 \theta \rangle$ (blue line). The simulated distributions of the rotational wave packet at the alignment and antialignment revivals are also presented.

microchannel plate and the supplied voltage, the detection efficiency of our detectors to detect one ion or electron is about 0.5. The higher electron rate as compared to the ion rate is due to the fact that the detected electrons are not only from the single-ionization event but also from double-ionization events where two electrons are produced for one doubly charged molecular ion, and the ionization event involved the background where only electrons are detected. Since electron-ion coincidence requires both ion and electron to be detected, we acquire the data using the ion signal as the trigger, i.e., the event is recorded when there is one hit on the ion detector. By using a momentum conservation gate along the time-of-flight direction of $|p_{z,C_2H_2^+} + p_{z,e}| < 0.5$ a.u. for the $C_2H_2^+$ and the correlated electron, we directly estimated the false electron-ion coincidence to be less than 25% in our measurement for this nondissociative single-ionization channel. Based on the relative systematic error of the coincidence data acquisition [22] for the $C_2H_2^+$ and (C_2H^+, H) channels, we deduced that the false coincidence rate for the (C_2H^+, H) channel is similar to that of $C_2H_2^+$. In addition to the (C_2H^+, H) channel, the double-ionization-induced Coulomb explosion channel of C_2H^+, H^+ is also observed, which shows a much larger kinetic energy release and therefore can be readily distinguished from the (C_2H^+, H) channel.

Driven by the femtosecond aligning pulse, the C_2H_2 with a rotational period of 14.2 ps is nonadiabatically aligned [23]. The field-free evolution of the impulsively excited rotational states leads to periodical revivals of alignment (along the y axis) or antialignment (confined in the $x-z$ plane) at well-defined time delays [10,24]. We characterized the alignment degree using the average term $\langle \cos^2 \phi \rangle$, where ϕ is the angle between the molecular axis and the field direction of the aligning pulse in the polarization plane of a time-delayed circularly polarized probe pulse. The molecular axis is extracted from the relative momentum of the ejected

fragmentized ions of the two-body Coulomb explosion channel of (CH^+, CH^+) . The events of the (CH^+, CH^+) channel are clearly selected from the measured data by using the two-ion coincidence condition, i.e., the momentum conservation of the two fragmentized ions. For a circularly polarized probe pulse, the isotropic molecular orientation corresponds to $\langle \cos^2 \phi \rangle = 0.5$; while the alignment and antialignment of the molecule result in $\langle \cos^2 \phi \rangle$ being larger and smaller than 0.5, respectively. The rotational temperature of the molecular beam is very close to the translation temperature [25], which can be experimentally estimated by $T_{\text{trans}} = \Delta p_y^2 / [4 \ln(4) k_B m]$. Here, k_B is the Boltzmann constant; Δp_y and m are the full width at half maximum (FWHM) of the momentum distribution in the jet direction and the mass of the singly ionized molecule, respectively. In our experiment we measure a momentum width in the jet direction of $\Delta p_y \sim 3.45$ a.u. of the $C_2H_2^+$ ion created by a laser pulse linearly polarized along the z direction. This results in an upper limit of the temperature of the C_2H_2 in the supersonic gas jet of ~ 14.2 K. As shown in the inset of Fig. 1, by setting the rotational temperature of 13 K, the numerically simulated arrival time of the first alignment maximum and other revivals match well with the experimental observations. It is also indicated by the broad revival structure that only a few rotational states are involved. As illustrated in the inset of Fig. 1, the time delay of the ionizing pulse was adjusted to be either $t_i = 6.7$ or 7.4 ps to match the alignment and antialignment revivals, respectively. To minimize the systematic errors caused by the fluctuation of the experimental parameters, we acquired the data for 10 s at each time delay and thereafter moved to the next one.

Although three-dimensional momenta of the freed electron were measured, in the following discussion we focus on the lateral momentum, i.e., the (p_x, p_y) projection for a z -polarized ionizing pulse which carries the fingerprint of the ionizing orbital and meanwhile is not streaked by the oscillating laser field of the ionizing pulse. Here, about 4.9×10^7 and 7.8×10^5 events were acquired for the $C_2H_2^+$ and (C_2H^+, H) channels, respectively. Figures 2(a) and 2(b) display the (p_x, p_y) projections of the freed electrons measured in coincidence with the $C_2H_2^+$ at $t_i = 6.7$ (alignment) or 7.4 (antialignment) ps, respectively. The lateral momenta are dominated by the filter effect of the laser-field-dressed potential barrier as predicted by the tunneling theory $\Psi_i(p_\perp) \sim \langle p_\perp | \Psi_i \rangle \exp(-\zeta p_\perp^2)$ [19,26,27], where Ψ_i is the field-free molecular orbital, and ζ is a parameter determining the filter strength. To exclude the tunneling filter and extract the orbital information carried by the lateral momentum of the directly freed electron, we differentially normalized the electron spectra by $(p_x, p_y)_{\text{norm}} = [(\langle p_x, p_y \rangle_{\text{align}} - \eta \langle p_x, p_y \rangle_{\text{antialign}})] / [\langle p_x, p_y \rangle_{\text{align}} + \eta \langle p_x, p_y \rangle_{\text{antialign}}]$, where $\eta = Y_{\text{align}} / Y_{\text{antialign}}$ is the yield ratio of the electrons from the aligned and antialigned molecules. As displayed in Fig. 2(c), a clear pattern is observed in the low-energy region of the normalized momentum distribution (enclosed in the dashed circle) as compared to the initial ones. These low-energy electrons directly escape to the continuum without additional interaction with the parent ion, standing for the “clean” electron to reveal the structure of the ionizing orbital. As shown in Fig. 2(d), a distinct pattern is observed in the normalized lateral momentum distribution of the

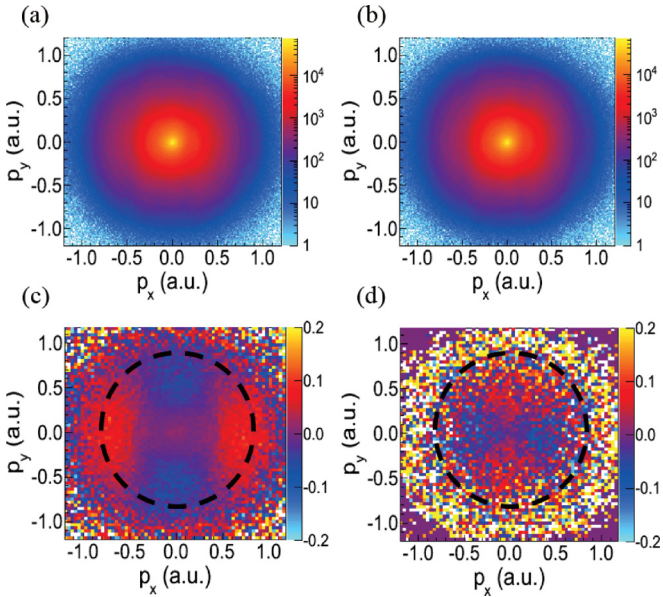


FIG. 2. (Color online) Lateral momentum distributions (p_x, p_y) of the freed electrons from the (a) aligned and (b) antialigned molecules measured in coincidence with the $C_2H_2^+$. The normalized difference $(p_x, p_y)_{\text{norm}}$ is displayed in (c). (d) Normalized difference $(p_x, p_y)_{\text{norm}}$ of the freed electrons measured in coincidence with the (C_2H^+, H) channel. The units of the color bar are counts in (a) and (b), and arbitrary in (c) and (d). The average bin content in (a) and (b) is about 635 counts per bin with a bin size of 0.012 a.u. The bin size is increased to 0.036 a.u. in (c) and (d) to enhance the visibility of the normalized difference.

freed electron measured in coincidence with the (C_2H^+, H) channel, indicating the participation of a different orbital as compared to the $C_2H_2^+$ molecular ion. It is consistent with recent observations [10] that the production of $C_2H_2^+$ and (C_2H^+, H) channels is favored when the molecule orients orthogonal or parallel to the polarization of the ionizing pulse, respectively, for which the $1\pi_u$ electron in HOMO or the $3\sigma_g$ electron in HOMO-1 is preferably removed. As compared to the orientation-dependent yield of the ions [10], here we directly reveal the participation of various orbitals for different ultimate channels by measuring the freed electrons in coincidence with the ions.

The ATI peaks in the photoelectron energy spectrum are shifted by the intensity-dependent ponderomotive energy. Considering the variation of the laser intensity and thus the ponderomotive energy in the interaction volume, the discrete ATI peaks are smeared out here as compared to results in previous work [11,28]. It is worth pointing out that after the removal of one HOMO electron, the ground $C_2H_2^+$ may be excited, and finally fragmentizes into the (C_2H^+, H) channel. Because of such sequential-excitation processes, the fragment-correlated MFPAD for this process does not have to coincide with that of the ground-state. For the possible sequential-excitation process, photons of less than 400 nm would be needed compared to the case of 800 nm pulses; thus the MFPAD is expected to be distinct. However, similar MFPADs are observed by comparing the electron momentum distribution triggered by either 800 nm or 400 nm pulses (see the following discussion). Therefore, we exclude a significant

contribution of this sequential-excitation process in the present work, if there is any.

Although the scenario of an imaginary orbital using direct electrons is developed in the tunneling ionization region which is usually triggered by NIR laser pulses of long wavelength, it is interesting to examine its validity using UV laser pulses in the intermediate regime with Keldysh parameter close to 1. It was demonstrated that the MFPAD is highly sensitive to the electronic state of the molecule for the few-photon ionization process [29]. Here, the UV pulse at 395 nm (z polarized) is generated by frequency-doubling a fundamental pulse at 790 nm in a 150- μm -thick β -barium borate (BBO) crystal, which was collinearly combined with the NIR aligning pulse and afterwards focused to singly ionize the molecule. The intensity of the UV ionizing pulse in the interaction region was measured to be $I_{i0} = 1.1 \times 10^{14} \text{ W/cm}^2$. Correspondingly, the Keldysh parameter for the UV pulse is calculated to be $\gamma = 1.9$, which is twice as large as that of the NIR pulse, $\gamma = 0.8$. For the UV ionizing pulse, about 4.9×10^7 and 6.0×10^5 events were acquired for the $C_2H_2^+$ and (C_2H^+, H) channels, respectively. Figures 3(a) and 3(b) display the (p_x, p_y) projections of the freed electron correlated with the $C_2H_2^+$ from the aligned and antialigned molecules, respectively. In spite of the similarity in Figs. 3(a) and 3(b), distinct patterns in the low-momentum region of the differentially normalized spectra $(p_x, p_y)_{\text{norm}}$ are clearly visible, as shown in Figs. 3(c) and 3(d). It hence validates the methodology of orbital imaging using direct electrons freed by a UV pulse. As compared to the NIR pulse, the momentum range of the direct electron carrying the orbital information is significantly reduced by using a UV pulse, characterized by its small ponderomotive potential.

In summary, we have experimentally observed distinct normalized lateral momenta of direct electrons from aligned and antialigned molecules in the strong-field single ionization of C_2H_2 , which are interpreted as a signature of multiple

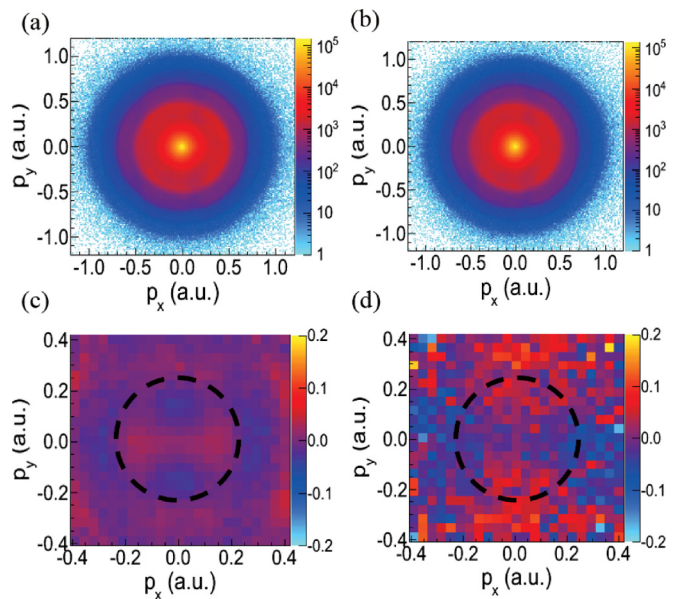


FIG. 3. (Color online) As Fig. 2 but for a UV ionizing pulse centered at 395 nm. The average bin content in (a) and (b) is about 619 counts per bin.

ionization orbitals. The validity of this scenario is verified using both NIR and UV ultrashort laser pulses with Keldysh parameter close to 1. Our findings demonstrate the possibility of distinguishing the participation of various orbitals in producing different channels in the strong-field single ionization of a polyatomic hydrocarbon molecule

We thank R. Dörner, C. D. Lin, and M. Meckel for helpful discussions. This work is supported by the National Natural Science Fund (Grants No. 11425416, No. 11374103, No. 11175120, and No. 11322438), the “Eastern Scholar” program, the NCET in University, and the “ShuGuang” Project (Grant No. 12SG25).

-
- [1] B. K. McFarland, J. P. Farrell, P. H. Bucksbaum, and M. Gühr, *Science* **322**, 1232 (2008).
- [2] H. Akagi, T. Otohe, A. Staudte, A. Shiner, F. Turner, R. Dörner, D. M. Villeneuve, and P. B. Corkum, *Science* **325**, 1364 (2009).
- [3] I. Znakovskaya, P. von den Hoff, S. Zherebtsov, A. Wirth, O. Herrwerth, M. J. J. Vrakking, R. de Vivie-Riedle, and M. F. Kling, *Phys. Rev. Lett.* **103**, 103002 (2009).
- [4] C. Wu, H. Zhang, H. Yang, Q. Gong, D. Song, and H. Su, *Phys. Rev. A* **83**, 033410 (2011).
- [5] J. Wu, L. Ph. H. Schmidt, M. Kunitski, M. Meckel, S. Voss, H. Sann, H. Kim, T. Jahnke, A. Czasch, and R. Dörner, *Phys. Rev. Lett.* **108**, 183001 (2012).
- [6] J. P. Yao, G. H. Li, X. Y. Jia, X. L. Hao, B. Zeng, C. R. Jing, W. Chu, J. L. Ni, H. S. Zhang, H. Q. Xie, C. J. Zhang, Z. X. Zhao, J. Chen, X. J. Liu, Y. Cheng, and Z. Z. Xu, *Phys. Rev. Lett.* **111**, 133001 (2013).
- [7] M. El-A. Madjet, O. Vendrell, and R. Santra, *Phys. Rev. Lett.* **107**, 263002 (2011).
- [8] Y. H. Jiang, A. Rudenko, O. Herrwerth, L. Foucar, M. Kurka, K. U. Kühnel, M. Lezius, M. F. Kling, J. van Tilborg, A. Belkacem, K. Ueda, S. Düsterer, R. Treusch, C. D. Schröter, R. Moshhammer, and J. Ullrich, *Phys. Rev. Lett.* **105**, 263002 (2010).
- [9] H. Ibrahim, B. Wales, S. Beaulieu, B. E. Schmidt, N. Thiré, E. P. Fowe, É. Bisson, C. T. Hebeisen, V. Wanie, M. Giguère, Jean-Claude Kieffer, M. Spanner, A. D. Bandrauk, J. Sanderson, M. S. Schuurman, and F. Légaré, *Nat. Commun.* **5**, 4422 (2014).
- [10] X. H. Xie, K. Doblhoff-Dier, H. L. Xu, S. Roither, M. S. Schöffler, D. Kartashov, S. Erattupuzha, T. Rathje, G. G. Paulus, K. Yamanouchi, A. Baltuška, S. Gräfe, and M. Kitzler, *Phys. Rev. Lett.* **112**, 163003 (2014).
- [11] A. E. Boguslavskiy, J. Mikosch, A. Gijsbertsen, M. Spanner, S. Patchkovskii, N. Gador, M. J. J. Vrakking, and A. Stolow, *Science* **335**, 1336 (2012).
- [12] X. M. Tong, Z. X. Zhao, and C. D. Lin, *Phys. Rev. A* **66**, 033402 (2002).
- [13] O. I. Tolstikhin, T. Morishita, and L. B. Madsen, *Phys. Rev. A* **84**, 053423 (2011).
- [14] J. Muth-Böhm, A. Becker, and F. H. M. Faisal, *Phys. Rev. Lett.* **85**, 2280 (2000).
- [15] M. Y. Ivanov, M. Spanner, and O. Smirnova, *J. Mod. Opt.* **52**, 165 (2005).
- [16] Y. H. Jiang, A. Senfleben, M. Kurka, A. Rudenko, L. Foucar, O. Herrwerth, M. F. Kling, M. Lezius, J. V. Tilborg, A. Belkacem, K. Ueda, D. Rolles, R. Treusch, Y. Z. Zhang, Y. F. Liu, C. D. Schröter, J. Ullrich, and R. Moshhammer, *J. Phys. B* **46**, 164027 (2013).
- [17] D. Pavičić, K. F. Lee, D. M. Rayner, P. B. Corkum, and D. M. Villeneuve, *Phys. Rev. Lett.* **98**, 243001 (2007).
- [18] I. Petersen, J. Henkel, and M. Lein, *Phys. Rev. Lett.* **114**, 103004 (2015).
- [19] M. Meckel, D. Comtois, D. Zeidler, A. Staudte, D. Pavičić, H. C. Bandulet, H. Pépin, J. C. Kieffer, R. Dörner, D. M. Villeneuve, and P. B. Corkum, *Science* **320**, 1478 (2008).
- [20] R. Dörner, V. Mergel, O. Jagutzki, L. Spielberger, J. Ullrich, R. Moshhammer, and H. Schmidt-Böcking, *Phys. Rep.* **330**, 95 (2000).
- [21] J. Ulrich, R. Moshhammer, A. Dorn, R. Dörner, L. Ph. H. Schmidt, and H. Schmidt-Böcking, *Rep. Prog. Phys.* **66**, 1463 (2003).
- [22] J. Mikosch and S. Patchkovskii, *J. Mod. Opt.* **60**, 17 (2013).
- [23] H. Stapelfeldt and T. Seideman, *Rev. Mod. Phys.* **75**, 543 (2003).
- [24] H. Li, W. Li, Y. Feng, J. Liu, H. Pan, and H. Zeng, *Phys. Rev. A* **85**, 052515 (2012).
- [25] J. Wu, A. Vredenburg, B. Ulrich, L. Ph. H. Schmidt, M. Meckel, S. Voss, H. Sann, H. Kim, T. Jahnke, and R. Dörner, *Phys. Rev. A* **83**, 061403(R) (2011).
- [26] A. S. Kheifets and I. A. Ivanov, *Phys. Rev. A* **90**, 033404 (2014).
- [27] L. Arissian, C. Smeenk, F. Turner, C. Trallero, A. V. Sokolov, D. M. Villeneuve, A. Staudte, and P. B. Corkum, *Phys. Rev. Lett.* **105**, 133002 (2010).
- [28] J. Mikosch, A. E. Boguslavskiy, I. Wilkinson, M. Spanner, S. Patchkovskii, and A. Stolow, *Phys. Rev. Lett.* **110**, 023004 (2013).
- [29] C. Z. Bisgaard, O. J. Clarkin, G. Wu, A. M. D. Lee, O. Geßner, C. C. Hayden, and A. Stolow, *Science* **323**, 1464 (2009).